Catalysis Letters Vol. 112, Nos. 3–4, December 2006 (© 2006)
DOI: 10.1007/s10562-006-0199-3

Studies on $CrO_x/La_2O_3/ZrO_2$ catalysts modified by Mg

D.L. Hoang,[a,*] S. Farage,[a] A. Dittmar,[a] A. Trunschke,[b] H. Lieske,[a] and A. Martin[a]

[a] *Leibniz-Institut für Katalyse e.V. an der Universität Rostock, Branch Berlin (former ACA), Richard-Willstätter-Str. 12, D-12489 Berlin, Germany*
[b] *Department of Inorganic Chemistry, Fritz-Haber-Institut der Max-Plack-Gesellschaft, Faradayweg 4-6, D-14195 Berlin, Germany*

Received 15 September 2006; accepted 4 October 2006

Lanthana–zirconia supported chromium oxide and magnesium chromium mixed oxide catalysts were studied in the dehydrocyclization of *n*-octane and characterized by temperature-programmed desorption of NH_3, temperature-programmed reduction, XPS and DRIFTS. The Mg-free catalyst shows the highest activity, but suffers from rapid deactivation due to coke formation. The addition of Mg decreases the initial activity of the supported chromium oxide and retards its deactivation. The characterization results reveal that the deactivation retarding effect of Mg species not only consists in the deletion of strong acid sites but also in the decoration and/or dilution of Cr^{3+} oxide cluster, supposedly due to the formation of Mg–Cr surface compounds and, thus, in preventing the formation of coke.

KEY WORDS: dehydrocyclization; lanthana–zirconia support; chromium oxide catalysts; chromium-magnesium-lanthanum oxide catalysts; catalyst characterization; coke deposition.

1. Introduction

Recently, we have found that $CrO_x/La_2O_3/ZrO_2$ (Cr/LZ) catalysts are able to catalyze the dehydrocyclization (DHC) of C_{6+} alkanes, exhibiting high selectivities for alkyl aromatics. At 773-823 K under hydrogen atmosphere the DHC of *n*-octane on Cr/LZ catalysts mainly produces o-xylene and ethylbenzene [1]. However, the strong deactivation of the catalysts due to coke deposition impedes an industrial application [2–4]. By means of *in-situ* ESR spectroscopy, the coexistence of catalytically active Cr^{3+} oxide clusters and isolated Cr^{3+} ions on the LZ support was revealed under reaction conditions. The isolated Cr species appeared to be less sensitive towards deactivation by coke deposition during the DHC of *n*-octane [4]. Therefore, our efforts were directed to suppress deactivation by coke formation by specific generation and stabilization of isolated Cr^{3+} species on the surface of the support.

Recently, we have suggested that strong interaction between La and Cr oxides could be responsible for stabilization of highly dispersed Cr species on the surface of Cr/LZ [5–7]. Magnesia is known to be able to interact with chromia or La-Cr mixed oxides resulting in $MgCr_2O_4$ with spinel structure or $LaCr_{1-x}Mg_xO_3$ with a substituted perovskite structure, respectively [8–10]. Moreover, MgO crystals, being simultaneously formed with La–Cr perovskite-type mixed oxide phases in oxidation catalyst systems, were proved to prevent sintering of the latter, keeping Cr containing species in a dispersed state [10]. On the other hand, MgO addition reduces the catalyst acidity that is known to promote coke formation leading to deactivation of the catalyst [7]. So, in the present study, chromia–lanthana–zirconia catalysts were modified by addition of magnesium oxide with the objectives to (i) diminish the catalyst acidity and to (ii) increase and/or stabilize the dispersion of Cr species in order to improve the stability of the catalyst system in the DHC of *n*-octane.

*To whom correspondence should be addressed.
E-mail: hoang@aca-berlin.de

2. Experimental

2.1. Catalyst preparation

A LZ material supplied by MEL Chemicals (Manchester, UK) was used as catalyst support. Cr/LZ was prepared by immersing LZ into an aqueous solution containing appropriate amount of $(NH_4)_2CrO_4$ as given below. By aqueous ammonia solution addition, the mixture was kept at pH 10. After evaporation of the solvent, the solid was dried at 353 K for 12 h and calcined at 873 K for 4 h.

Magnesia-containing Cr/LZ catalysts (Mg–Cr/LZ) were prepared by immersing the LZ support into an aqueous solution containing appropriate amounts of $(NH_4)_2CrO_4$ and $Mg(NO_3)_2$, as also given below. Again, the solutions were kept at pH 10 by aqueous ammonia solution addition. The drying and calcination procedure corresponds to that of the Mg-free catalyst.

The chromium content was 0.77 mmol Cr/g_{cat} in the Mg-free as well as in the Mg-containing catalysts. The Mg/Cr molar ratio has been varied between 0 and 5.0. Hereafter, the Mg-modified Cr/LZ catalysts will be denoted as (*x*)Mg–Cr/LZ, where (*x*) indicates the Mg/Cr molar ratio.

2.2. Catalytic test reaction

DHC of *n*-octane was carried out in a quartz reactor containing 500 mg catalyst with grain size fraction of 0.3–0.8 mm under normal pressure at 823 K. Hydrogen (flow rate = 3.0 l/h), saturated with *n*-octane at 303 K ($p_{n\text{-octane}}$ = ca. 3.1 kPa) was applied as feed. The reaction products were analyzed by on line-GC that was equipped with a 50 m PONA capillary column.

2.3. Catalyst characterisation

The specific surface areas (BET, m^2/g_{cat}) of the calcined catalysts have been determined by nitrogen adsorption at 77 K, using a BET surface analyzer NOVA-1200 (Quantachrome).

NH_3–TPD was performed in a characterization apparatus RIG-100 (In-Situ Research & Instruments), consisting of a fixed-bed quartz reactor and a gas analysis system. Before the TPD measurements, the samples were reduced in hydrogen flow at 823 K for 2 h. After cooling the solid in a helium flow to 373 K, ammonia was adsorbed at this temperature. The following desorption of NH_3 was carried out in a helium flow, with a flow rate of 15 ml/min and at a heating rate of 10 K/min.

The TPR procedure has been described in detail in [11]. The calcined samples, with a particle size of 0.3–0.8 mm, were placed into the reactor and heated in an argon flow at 573 K for 1 h before TPR measurement. Optimum sample weights had been estimated according to Monti and Baiker [12]. After cooling the sample in the argon flow to 323 K, the first TPR run, TPR1, was carried out in a 5.17% hydrogen in argon flow at a gas flow rate of 15 ml/min and at a heating rate of 10 K/min. Hydrogen consumed, quantitatively determined as mmol H_2/g_{cat}, during TPR run was monitored by a thermal conductivity detector (GOW-MAC Instruments). TPR1 was finished by an isothermal period at 1023 K, which was followed by a reoxidation in He flow containing 20% O_2 at 873 K for 1 h. Afterwards, the second TPR run, TPR2, was carried out under the conditions of TPR1.

Diffuse Reflectance Infrared Fourier Transform (DRIFT) spectra were recorded on a spectrometer FTS-60 A (BIO-RAD) accumulating 256 scans at 2 cm^{-1} resolution. The *ex-situ* calcined samples were placed in the reaction chamber of a diffuse reflectance attachment (HARRICK) and treated in N_2 flow (20 ml/min) at 573 K for 1 h. Thereafter, the samples were reduced at 823 K for 1 h in a H_2/N_2 mixture containing 20 vol.% H_2, evacuated at 823 K for 30 min and cooled down to 298 K. The adsorption of NO was carried out at 298 K by consecutively adding NO with partial pressures of 0.1, 0.5, 1.0, 2.0, 5.0 7.5, 10.0 and 20.0 mbar, respectively. The spectra were recorded at 313 K and presented in Kubelka–Munk mode, referring to a KBr background spectrum.

X-Ray Photoelectron spectra (XPS) were recorded on a SAGE 100 spectrometer (SPECS) using a non-monochromatized MgKα source operating at 20 mA and 12.5 kV. In the case of Cr/LZ and (*x*)Mg–Cr/LZ samples, the Zr $3d_{5/2}$ peak with the binding energy of 182.2 eV was used as reference. The XPS peaks were fitted with Gauss–Lorentz curves. For quantitative analysis, the areas below the peaks were determined with SPECS software after subtracting a Shirley background. The intensity ratios of the $Cr2p_{3/2}$ and Mg2p to the Zr $3d5_{5/2}$ nominated peaks, I_{Cr}/I_{Zr} and I_{Mg}/I_{Zr}, respectively, were calculated and used as measures of the relative near-surface concentrations of Cr in the Cr/LZ sample as well as of Cr and Mg in (*x*)Mg–Cr/LZ [7].

3. Results and discussion

3.1. DHC of n-octane

In figure 1, *n*-octane conversion on LZ, Cr/LZ and (*x*)Mg–Cr/LZ is shown as a function of time-on-stream (TOS). A comparison of the product selectivities after 180 min TOS is depicted in figure 2. As earlier reported [7], LZ support itself shows some catalytic activity. Figure 1 and table 1 also demonstrate that this activity seems to be stable during the TOS tested and that the amount of coke formed is rather low. The reason for the activity of LZ is supposedly related to Zr^{3+} sites formed by hydrogen treatment of LZ support [13]. The distribution of the products obtained on LZ shows that o-xylen and ethylbenzene are the main products among aromatics (figure 2). This suggests a DHC mechanism based on a stepwise dehydrogenation, alkane → alkene → alkadiene → alkatrienen → cyclohexadiene → aromatics, which had been found to be characteristic for the DHC of alkanes on catalysts of non-acidic nature [14–17]. The *n*-octane conversion on Cr/LZ is high at the very beginning, in agreement with the results reported in [2,3], but it decreases rapidly. The catalytic activity of

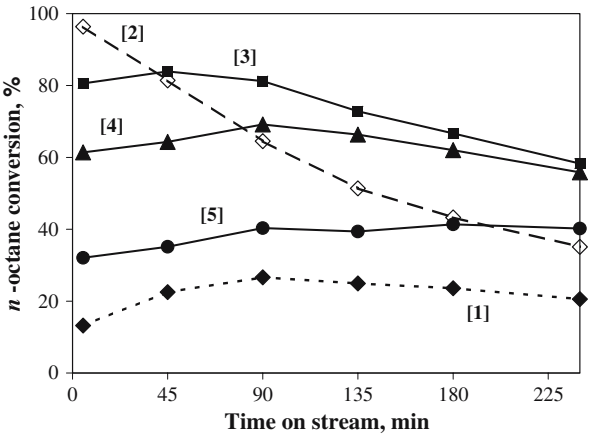

Figure 1. *n*-octane conversion as function of time on stream: LZ [1], Cr/LZ [2], (0.5)Mg–Cr/LZ [3], (1.1)Mg–Cr/LZ [4], (2.2) Mg–Cr/LZ [5].

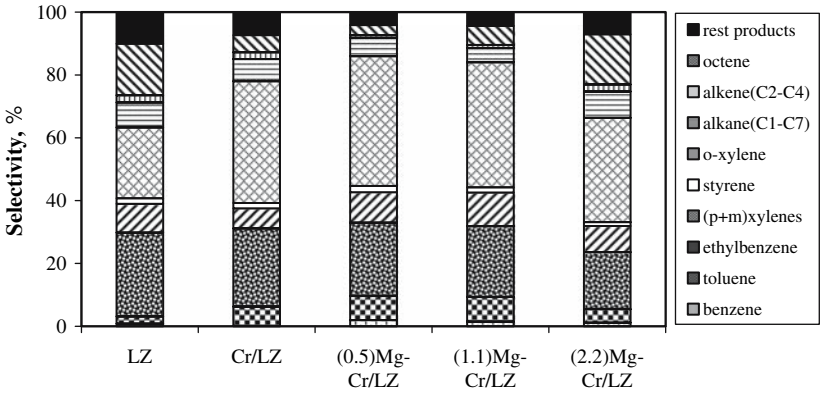

Figure 2. Product selectivity of LZ support and Cr/LZ and (*x*)Mg–Cr/LZ catalysts after 180 min on stream.

Table 1
Specific surface areas (BET), amount of NH_3 desorption ($mmolNH_3/g_{cat}$), surface density of acid sites ($mmolNH_3/m^2$) and deposited coke amounts (wt.-%) after catalytic runs

Catalyst	BET m^2/g_{cat}	NH_3 desorption mmol NH_3/g_{cat}	Surface density mmol $NH_3/m^2.10^{-4}$	Carbon content wt.-%
LZ	102.0	0.09		0.7
Cr/LZ	147.5	0.24	16.27	3.6
(0.5)Mg–Cr/LZ	125.4	0.14	11.0	0.7
(1.1)Mg–Cr/LZ	103.7	0.12	11.19	–
(2.2)Mg–Cr/LZ	87.2	0.11	12.61	0.9

Cr/LZ has been assigned to Cr^{3+} sites [2–4,7]. In [2], we have reported that the decrease in *n*-octane conversion on Cr/LZ is associated with a slight decrease in the selectivity to aromatics. However, at 180 min TOS, aromatics still were the predominating products, mainly consisting of ethylbenzene and o-xylene as shown in figure 2. This suggests that the presence of Cr^{3+} species does not significantly affect the stepwise dehydrogenation mechanism assumed above for the DHC of *n*-octane on LZ [14–17]. Further, while the product distribution is only moderately influenced by modification of the Cr/LZ catalyst with Mg, activity and deactivation behaviour are strongly affected. Figure 1 also shows that the initial *n*-octane conversion on the Mg-containing catalysts is lower than on the Mg-free Cr/LZ. With increasing TOS, the conversion strongly decreases over Cr/LZ, while over the Mg-containing catalysts, the conversion remains almost unchanged. This result reveals the dual impact of the Mg addition consisting, on the one hand, in lowering the initial *n*-octane conversion and, on the other hand, in retarding the deactivation of the Cr/LZ parent catalyst. This influence depends on the Mg loading, namely, the higher the Mg content, the lower the initial activity and the higher the stability (cf. figure 1). With Cr/LZ catalysts, we have found evidence for coke deposition as the main reason for catalyst deactivation during *n*-octane DHC [2–4]. So, the higher stability of (*x*)Mg–Cr/LZ catalysts suggests a retardation of coke deposition on them during the DHC reaction. Actually, the results of the C-H analysis carried out with used catalysts after 240 min TOS (cf. table 1) shows that the carbon content is 3.6 wt.% for Cr/LZ and ca. 1 wt.% for the Mg-containing catalysts only, i.e., as low as the carbon content obtained for the pure support LZ after the catalytic test.

Coke formation on Cr containing catalysts, as known, may proceed on acid sites [18] and/or on large chromium dioxide clusters [2,4,7]. The observed retardation of coke formation on (*x*)Mg–Cr/LZ catalysts can, therefore, be caused (i) by diminishing the acidity of Cr/LZ due to the Mg addition and/or (ii) by an influence of Mg on the dispersion of Cr oxide species. We studied the catalyst acidity by NH_3–TPD, and the Cr oxide dispersion by TPR, DRIFTS and XPS, respectively.

3.2. NH_3–TPD

The total amount of acid sites on LZ, Cr/LZ and (*x*)Mg–Cr/LZ is given in table 1 together with the specific surface areas. The desorption profiles of ammonia are shown in figure 3.

As found in [7], the LZ support and Cr/LZ catalyst exhibit only low Lewis acidity. The maximum of NH_3 desorption from LZ is recorded at low temperatures between 473 and 523 K (cf. figure 3) being characteristic for weak acid sites. The Cr loading significantly increases the number of acid sites on Cr/LZ catalyst (table 1) as well as their strength, indicated by the NH_3 desorption at higher temperatures of around 650 K. Thus, comparing the results of catalytic test (figure 1) and the amount of coke formed on the LZ support and on the Cr/LZ catalyst (table 1), it seems that Cr species were responsible for stronger acidity of Cr/LZ and, therefore, for its higher activity in DHC as well as higher deactivation rates. Furthermore, the NH_3–TPD profiles of the Cr/LZ and (*x*)Mg–Cr/LZ catalysts in figure 3 reveal that the addition of Mg completely erases the high-temperature signal of strong acid sites, without significantly affecting the intensity of the low-temperature one of weaker acid sites.

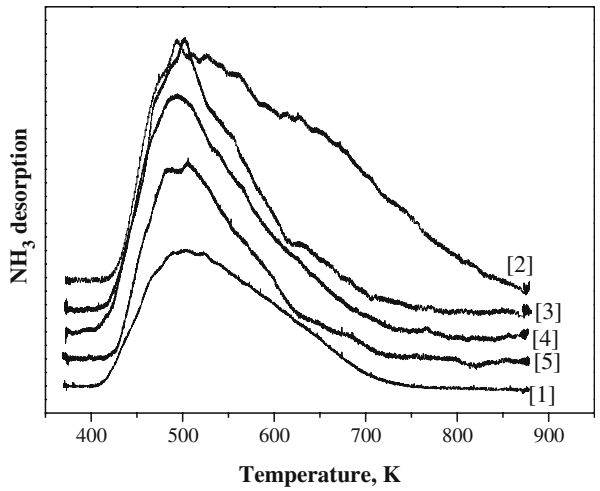

Figure 3. NH_3–TPD profiles of LZ [1]; Cr/LZ [2]; (0.5)Mg–Cr/LZ [3]; (1.1)Mg–Cr/LZ [4]; (2.2)Mg–Cr/LZ [5].

This gives hints on a Mg–Cr interaction that neutralizes the strong acid sites. Figure 1 and table 1 show, on the other hand, that the initial activity, the deactivation rate of the Cr/LZ catalyst as well as the amounts of coke formed on it similarly decrease with the addition of Mg. This supports once more the suggestion that strong acid sites were responsible for high initial activity as well as for the dramatic deactivation of Cr/LZ.

However, as shown above (figure 2), the distribution of the products obtained on Cr/LZ is not significantly different from the one on LZ. This, as mentioned above, suggests that the acidity enhanced by Cr species does not significantly change the stepwise dehydrogenation mechanism assumed above for the *n*-octane DHC on LZ. The addition of Mg with increasing loading does not change product distribution as well. Moreover, as can be seen from table 1, although the total number of acid sites is decreased with increasing Mg loading on Cr/LZ, but the specific surface area also decreases in parallel, so that the surface density of acid sites (mmol NH_3/m^2) remains roughly unchanged. While strong acid sites completely disappear with the first portion of Mg, corresponding to Mg/Cr molar ratio of 0.5, the (*x*)Mg–Cr/LZ catalysts remain still more active than the pure LZ support.

Thus, all these results show that the catalytic behaviour of (*x*)Mg–Cr/LZ catalysts hardly depend only on amount and strength of the acid sites. It is more reasonable to suggest that the observed catalytic differences among the Mg-free and the Mg-containing catalysts rather arise from changes of the nature of Cr species as active sites or of their dispersion. In the following, this is examined by TPR, DRIFTS and XPS studies.

3.3. TPR

The TPR1 and TPR2 profiles obtained for Cr/LZ and (*x*)Mg–Cr/LZ catalysts are shown in figure 4a and b,

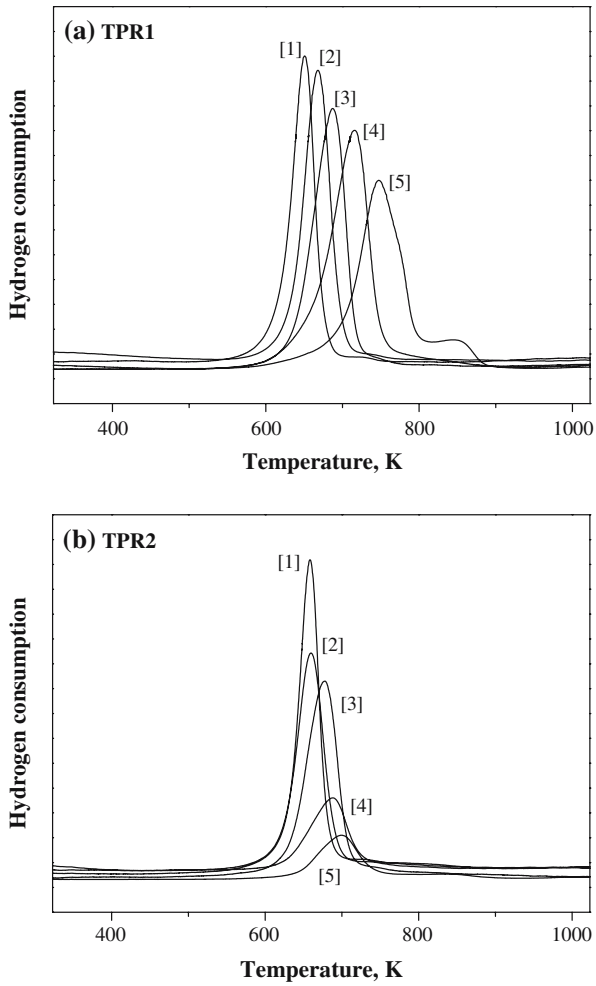

Figure 4. TPR1(a) and TPR2(b) profiles of Cr/LZ [1]; (0.5)Mg–Cr/LZ [2]; (1.1)Mg–Cr/LZ [3]; (2.2)Mg–Cr/LZ [4] and (4.7)Mg–Cr/LZ [5] catalysts.

respectively. The quantitative TPR1 and TPR2 results, including hydrogen consumption (mmol H_2/g_{cat}), T_{max} values and oxidation state changes (n−m) [5,6,11], are listed in table 2. With the Mg-free catalyst, no differences between TPR1 and TPR2 have been observed with respect to peak area and T_{max} [11]. The hydrogen consumption measured in TPR1 and TPR2 correspond to an oxidation state change (n−m) of 2.5. As we discussed in [10], this deviation from the expected value "3" for reduction of Cr^{6+} to Cr^{3+} gives a hint on the existence of a small portion of Cr^{3+} formed by partial thermal decomposition of Cr(VI) oxide at higher temperatures [18]. However, the TPR results evidence a complete reoxidability of Cr^{3+} species to Cr^{n+}(n = 5–6) in the reoxidation treatment. In [5,6] we suggested the formation of La–Cr surface compounds to be responsible for this reversibility.

The TPR1 profiles of (*x*)Mg–Cr/LZ catalysts reveal that the modification of Cr/LZ with Mg strongly influences the reduction behaviour of Cr^{n+} species. Simultaneous reduction of Mg^{2+} can be excluded [8].

Table 2
Hydrogen consumption, T_{max} and oxidation state changes (n−m) during the TPR1 and TPR2

Catalyst	TPR1			TPR2		
	H_2 consumption $mmolH_2/g_{cat}$	T_{max} K	n−m	H_2 consumption $mmolH_2/g_{cat}$	T_{max} K	n−m
Cr/LZ	0.97	650	2.5	0.97	658	2.5
(0.5)Mg–Cr/LZ	0.78	667	2.0	0.58	660	1.5
(1.1)Mg–Cr/LZ	0.79	687	2.1	0.60	677	1.6
(1.7)Mg–Cr/LZ	0.85	699	2.2	0.70	682	1.8
(2.2)Mg–Cr/LZ	0.89	715	2.3	0.33	687	0.9
(4.7)Mg–Cr/LZ	0.80	746	2.1	0.21	698	0.6

With increasing Mg loading, the reduction temperature (T_{max}) is shifted to higher values (figure 4a and table 2). This shows an increasing interaction between Mg and Cr species that makes the reduction of Cr more and more difficult. Moreover, Mg addition causes strong deformations of the TPR1 profiles. However, the total hydrogen consumption is only slightly reduced by Mg addition. This becomes more apparent in figure 5, curve (a). The oxidation state changes (n−m) calculated from hydrogen consumption are nearly independent of the Mg loading and range between 2.0 and 2.3. As in the case of the Mg-free catalyst, this may correspond to the reduction of Cr^{n+} (n = 5–6) to Cr^{3+}. Hence, although Mg obviously strongly interacts with Cr^{n+} species and impedes their reduction, it leaves the initial oxidation state of Cr almost unchanged. Unlike the Mg-free catalyst Cr/LZ, the TPR2 profiles of the Mg-containing catalysts (x)Mg–Cr/LZ show that Cr^{n+}(n = 5–6) species, reduced by TPR1 to Cr^{3+}, are not completely restored by reoxidation (figure 4b). The TPR2 hydrogen consumption listed in table 2 and depicted in figure 5, curve (b), confirm this and clearly show that the fraction of reoxidable Cr species drastically decreases with increasing Mg loading. In accordance with this finding, the (n−m) values listed in table 2 strongly deviate from the expected value of n−m = 3. Bearing in mind that the reoxidability of Cr in Mg-free Cr/LZ has been attributed to the formation of La–Cr surface compounds [5,6], the diminished reoxidability of Cr in the (x)Mg–Cr/LZ catalysts suggests that Mg hampers or prevents the formation of such compounds. The amount of reoxidable Cr species decreases in the following order: Cr/LZ > (0.5)Mg–Cr/LZ > (1.1)Mg–Cr/LZ > (2.2)Mg–Cr/LZ > (4.7)Mg–Cr/LZ (table 2). This is consistent with the order of initial activities in *n*-octane conversion (cf. figure 1). Hence, a correlation between the amount of reoxidable Cr^{3+} species and catalytic activity is suggested. According to [11], a high dispersion is crucial for reoxidability of Cr^{3+} species. Moreover, high dispersion was found to suppress deactivation [4]. However, although in the Mg-free catalyst Cr/LZ the highest portion of reoxidable Cr^{3+} exists, it was deactivated more rapidly than Mg-containing catalysts. This shows that the dispersion of Cr^{3+} species is not the only parameter affecting the catalytic stability.

3.4. DRIFTS

Figure 6 depicts the DRIFT spectra of Cr/LZ and (x)Mg–Cr/LZ catalysts upon exposure to 10 mbar NO at 298 K. With Cr/LZ, bands at 2230, 2202, 1832, 1685 and 1200 cm^{-1} are observed. Due to the complex nature of the catalyst surface, an unambiguous assignment of the peaks is difficult. Disproportionation of NO is indicated by the appearance of bands at 2230 and 2202 cm^{-1} due to N–N stretching vibrations of N_2O, presumably adsorbed on two different surface sites. The intense band at 1685 cm^{-1} and the one at 1200 cm^{-1} are assigned to the splitted v_3 mode of bridging bidentate nitrate species [19]. The band at 1832 cm^{-1} could be attributed to the symmetric stretching mode of chromium dinitrosyls [7], however, shifted to lower wavenumbers compared to the spectra typically measured upon NO adsorption on Cr/ZrO_2 [19]. The

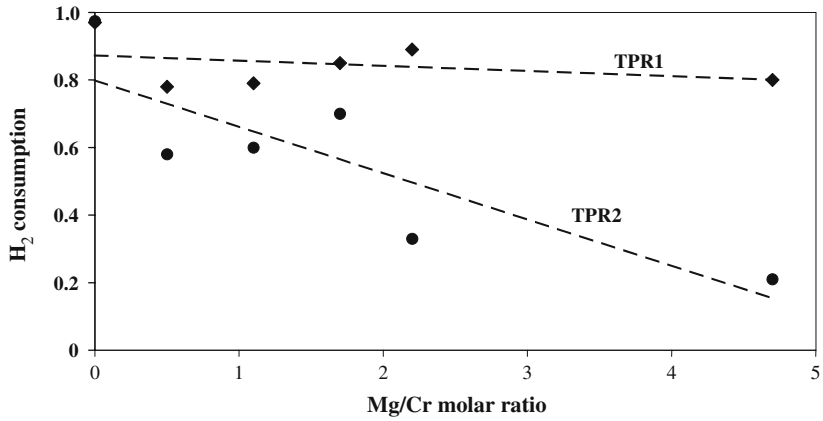

Figure 5. H_2 consumption during TPR1 and TPR2 as function of Mg/Cr molar ratio.

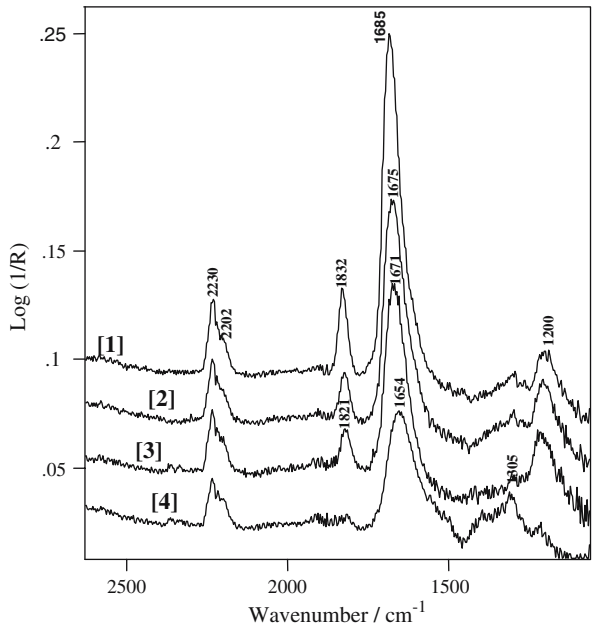

Figure 6. DRIFT spectra of Cr/LZ [1] and (0.5)Mg–Cr/LZ [2], (1.1]Mg–Cr/LZ[3] and (2.2)Mg–Cr/LZ catalysts.

corresponding asymmetric stretching mode overlaps with the band due to surface nitrate at 1685 cm^{-1}. With increasing Mg loading, a shift of the symmetric stretching mode of the dinitrosyl complex to lower energies is observed (figure 6). Moreover, the band intensity decreases until, finally, the band disappears on (2.2)Mg–Cr/LZ. NO is known to be a selective probe of coordinatively unsaturated (*cus*) chromium ions, in particular those with two coordination vacancies, on the surface of lanthana-containing zirconia [7]. The fact that the increase of Mg loading shifts the frequency of the symmetric stretching mode to lower energies and decreases the band intensity may, therefore, indicate a change of the nature of *cus*-Cr ions on the surface due to Mg–Cr-oxide interactions and/or due to coverage of coordinatively unsaturated chromium species by Mg. This seems to support the suggestion made above by the NH_3–TPD experiments. We further examined the oxidation states and the near-surface concentration of Cr as well as Mg cations in the Cr/LZ and (*x*)Mg–Cr/LZ catalysts by means of XPS.

3.5. XPS

Figure 7 (a, b) shows the XPS spectra of Cr/LZ and (2.2)Mg–Cr/LZ, respectively, after calcination as well as after TPR2. The broad peak with a $2p_{3/2}$ binding energy (BE) of ca. 579 eV in the spectrum of calcined Cr/LZ (curve 1 in figure 7a) characterizes Cr in oxidation state +6. The small shoulder that appears at lower BE is assigned to Cr^{n+} species, where $3 < n < 6$ [7]. Like TPR results, this indicates that a part of Cr^{6+} species is already decomposed during the catalyst calcinations [18]. In accordance with the TPR1 results (cf. table 2),

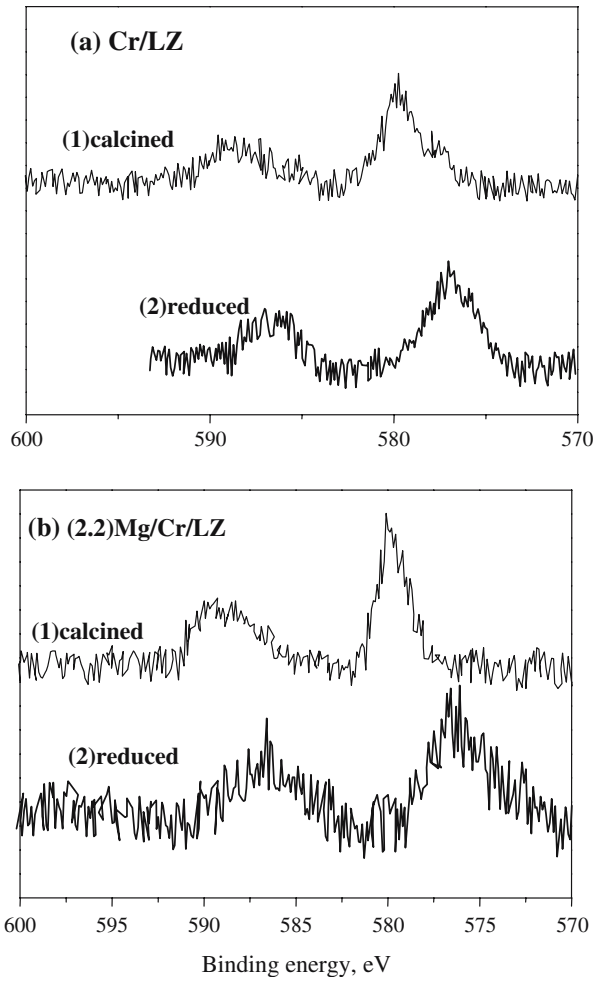

Figure 7. XPS spectra of Cr/LZ (a) and (2.2)Mg–Cr/LZ catalysts (b).

the portions of Cr^{6+} and Cr^{n+} can be estimated as ca. 70% and 30%, respectively, by peak fitting. After TPR2, the XPS spectrum of Cr/LZ (curve 2 in figure 7a) reveals a symmetric peak with BE of 576.9 eV, characterizing Cr ions in oxidation state +3, and the disappearance of the Cr^{6+}/Cr^{n+} signal. This indicates, in agreement with TPR, a complete reduction of Cr^{6+}/C^{n+} species in Cr/LZ to Cr^{3+} [10].

The XPS spectrum of calcined (2.2)Mg–Cr/LZ (curve 1 in figure 7b) shows a symmetric peak at 579 eV characteristic for Cr^{6+} species without the shoulder at lower binding energies. Evidently, Mg addition stabilizes chromium in the highest oxidation state during calcination. In reduced (2.2)Mg–Cr/LZ sample, the peak with BE of 576.9 eV (curve 2 in figure 7b) indicates the presence of only Cr^{3+} species. So, the XPS experiments do not evidence any possible changes of the oxidation state of Cr species on (*x*)Mg–Cr/LZ due to Mg–Cr-oxide interactions supposed above by DRIFTS and NH_3–TPD measurements.

Figure 8a and b depict the peak intensity ratios, I_{Cr}/I_{Zr} and I_{Mg}/I_{Zr}, representing the relative near surface concentration of chromium and magnesium, respec-

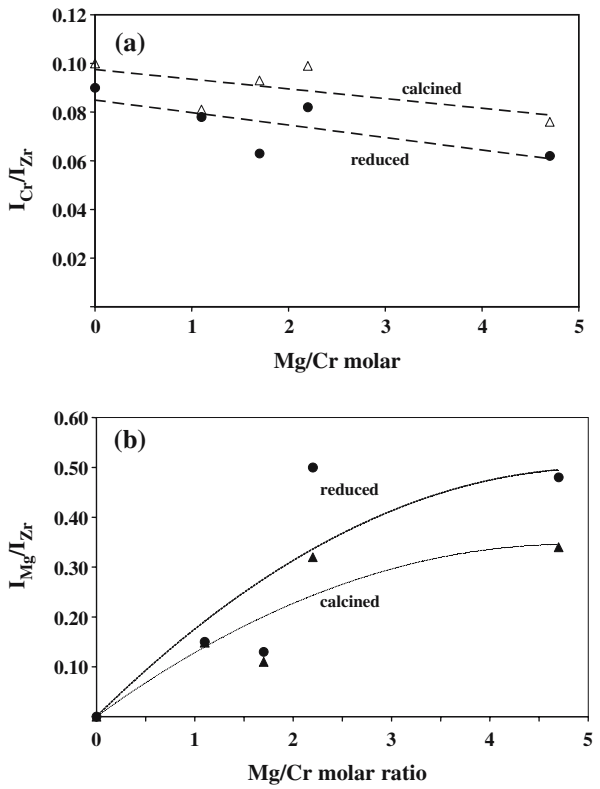

Figure 8. I_{Cr}/I_{Zr} (a) and I_{Mg}/I_{Zr} (b) as function of Mg/Cr molar ratio.

tively, as a function of the bulk Mg/Cr molar ratio. The I_{Cr}/I_{Zr} ratios of the calcined (*x*)Mg–Cr/LZ catalysts are only slightly lower than in Cr/LZ and remain almost constant with increasing Mg loading. No significant changes are observed after reduction indicating that the dispersion of chromium remains almost unchanged. The I_{Mg}/I_{Zr} ratios at lower Mg loadings are almost independent of the treatment conditions (figure 8b). With Mg/Cr molar ratios > 2, however, the reduction clearly enhances the I_{Mg}/I_{Zr} ratio. These XPS findings seem, on the one hand, to be in agreement with the DRIFTS results hinting on an accumulation of Mg on the surface. On the other hand, however, they are in contradiction to the TPR results, which revealed that the reoxidable portion of Cr species drastically decrease with increasing Mg loading (cf. figures 4b and 5). Because these reoxidable species should be highly dispersed [11], a strong decrease of them would strongly lower the I_{Cr}/I_{Zr} ratios. The contradiction between the TPR and XPS results can be explained by assuming a formation of Mg–Cr mixed oxide compounds in the near surface region, which are non-reoxidable but contain dispersed Cr species in oxidation state +3. Such compounds may be of the spinel-type as $MgCr_2O_4$ and/or of the perovskite-type as $LaCr_{1-x}Mg_xO_3$ [8–10]. In such mixed oxide systems, Cr species exist in the oxidation state $\leq +3$. This is in line with our DRIFTS experiments. Moreover, the formed mixed oxides would be located on the surface among reoxidable Cr^{3+} clusters, so that the I_{Cr}/I_{Zr} ratios determined by XPS remain almost unchanged (figure 8a). The identification of such mixed oxides will be the objective of our studies in the near future.

The thesis of the existence of Mg–Cr mixed oxide surface compounds enables to explain the catalytic behaviour of Cr/LZ and (*x*)Mg–Cr/LZ catalysts. The reason for the deactivation of Cr/LZ consists, as shown in [2–4], in the coverage of Cr^{3+} active sites by coke of aromatic nature. The coke formation happens on strong acid sites and is, moreover, facilitated by the presence of large Cr_2O_3 clusters and/or agglomerates of active Cr^{3+} species [4]. As evidenced by NH_3–TPD, the strong acidity in Cr/LZ is deleted by addition of small amounts of Mg leading to lower initial activity, drastically reduced coke formation and, therefore, retarded catalyst deactivation. With increasing Mg content, the lifetime of the catalyst is further increased by the formation of Mg–Cr mixed surface oxides that dilute large ensembles of active Cr^{3+} species and, by this way, additionally prevent coke formation. Thus, the effect of Mg species to retarding coke formation seems to act in a similar way as the known ensemble effect in case of metal catalysts [20].

4. Conclusions

Cr/LZ and (*x*)Mg–Cr/LZ catalysts were studied in the dehydrocyclization of *n*-octane and characterized by NH_3–TPD, TPR DRIFTS and XPS. The Mg-free catalyst shows the highest activity, but suffers from strong deactivation due to coke formation. The addition of Mg neutralizes strong acid sites and, in consequence, decreases the initial activity of Cr/LZ but retards its deactivation. This effect increases with increasing Mg loading. The stability of the Mg-containing catalysts is suggested to be additionally improved by decorating and/or diluting impacts of Mg species that, due to the formation of Mg–Cr mixed oxides, prevent the agglomerations of active Cr^{3+} species and, therefore, the accumulation of coke thereon.

Acknowledgments

Financial support by the Federal Ministry for Education and Research of the Federal Republic of Germany (project 03C3013), the EU (European Fund for Regional Developement) and the federal state of Berlin (Department for Science, Research and Culture) is gratefully acknowledged. The authors are responsible for the contents. The authors are thankful to Mrs. W. Ziesche for technical supports.

References

[1] H. Lieske and D.L. Hoang, US Patent 6 239 323 (2001).
[2] D.L. Hoang, A. Trunschke, A. Brückner, J. Radnik and H. Lieske, in: *Studies in Surface Science and Catalysis*, Vol. 130, eds.

A. Corma, F.V. Melo, S. Mendioroz and J.L. Fierro (Elsevier, Amsterdam, 2000) p. 2357.
[3] H. Ehwald, D.L. Hoang, U. Leibnitz and H. Lieske, in: *Studies in Surface Science and Catalysis*, Vol. 139, eds. J.J. Spivey, G.W. Roberts and B.H. Davis (Elsevier, Amsterdam, 2001) p. 117.
[4] A. Brückner, J. Radnik, D.L. Hoang and H. Lieske, Catal. Lett. 60 (1999) 183.
[5] D.L. Hoang, A. Dittmar, J. Radnik, K.-W. Brzezinka K. Witke, Appl. Catal. A: General 239 (2003) 95.
[6] D.L. Hoang, A. Dittmar, M. Schneider, A. Trunschke, H. Lieske, K.-W. Brzezinka and K. Witke, Thermochim. Acta 400 (2003) 153.
[7] A. Trunschke, D.L. Hoang, J. Radnik and H. Lieske, J. Catal. 191 (2000) 456.
[8] F.A. Cotton and G. Wilkinson, *Advanced Inorganic Chemistry* (John Wiley & Sons, Inc., 1962).
[9] E. Finochio, G. Ramis, G. Busca, V. Lorenzelli and R.J. Willey, Catal. Today 28 (1996) 381.
[10] G. Saracco, G. Scibilia, A. Iannibello and G. Baldi, Appl. Catal. B: Environmental 8 (1996) 229.
[11] D.L. Hoang and H. Lieske, Thermochim. Acta 345 (2000) 93.
[12] D.A.M. Monti and A. Baiker, J. Catal. 83 (1983) 323.
[13] S. Farrage, Ph.D. Thesis (Humboldt Universität Berlin, 2005).
[14] Z. Paál, Adv. Catal. 29 (1983) 273.
[15] B.H. Davis and P. Venuto, J. Catal. 15 (1969) 363.
[16] O. Klepel, C. Breitkopf and M. Standke, J. Mol. Catal. A: Chemical 210 (2004) 211.
[17] C. Breitkopf and O. Klepel, J. Mol. Catal. A: Chemical 211 (2004) 111.
[18] B.M. Weckhuysen, I.E. Wachs and R.A. Schonheydt, Chem. Rev. 96 (1996) 3327.
[19] K.I. Hadjiivanov, Catal. Rev.-Sci. Eng. 42 (2000) 71.
[20] J.H. Sinfelt, J. Catal. 29 (1973) 308.